THE JOURNAL OF PHYSICAL CHEMISTRY C

Article

Cite This: J. Phys. Chem. C 2019, 123, 62−69

pubs.acs.org/JPCC

Elucidating the Role of Temperature and Pressure to the Thermodynamic Stability of Charged Defects in Complex Metal-Hydrides: A Case Study of $NaAlH_4$

Ekta Arora,* Shikha Saini, Pooja Basera, Manish Kumar, Arunima Singh, and Saswata Bhattacharya*

Department of Physics, Indian Institute of Technology Delhi, New Delhi 110016, India

ABSTRACT: Complex metal hydrides are one of the most technologically relevant classes of hydrogen storage materials because of their huge applications as clean energy alternatives. In this class of materials, hydrogen-related point defects have been shown to play a crucial role in catalyzed dehydrogenation. We investigate the effects of environment (viz. finite temperature, hydrogen partial pressure, and doping) to understand the thermodynamic stability of point defects as a function of various charge states at a realistic condition in a bulk complex metal-hydride, using $NaAlH_4$ as an example. Our approach employs density-functional theory (DFT) combined with ab initio atomistic thermodynamics, where the free energy of formation due to vibration of phonons is duly considered under harmonic approximation. We show that to understand the thermodynamic stability of various defects and its self-diffusion, the contribution of environmental effect to the free energy of formation is absolutely indispensable. We further validate that DFT with appropriate exchange and correlation functionals fails to predict the stable phases even at a moderately low temperature.

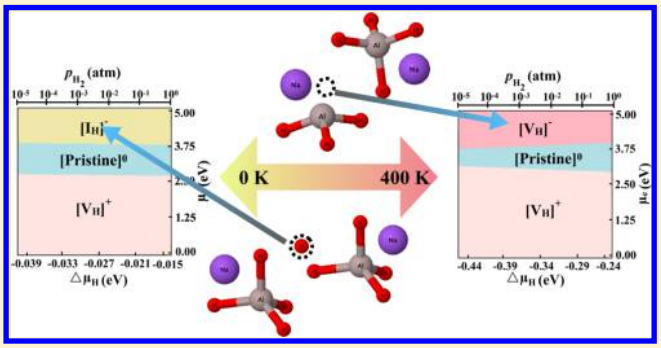

INTRODUCTION

Complex metal hydrides are a promising class of materials. It is rapidly expanding with various multifunctionality, having applications in particular within the field of energy storage.[1−5] In past, much attention has been devoted to aluminum-based hydrides, in particular to alanates (hydridoaluminates).[2,3,6,7] These compounds can store a significant amount of hydrogen and some are also reversible at rather moderate conditions. One important example is sodium alanate ($NaAlH_4$).[8] Despite very interesting studies in the past on desorption kinetics in catalyzed $NaAlH_4$,[9,10] the catalytic effect of metal additives on the kinetics of hydrogen adsorption/desorption is not well understood at the microscopic level. It is usually believed that intrinsic point defects play a decisive role in catalyzing the dehydrogenation in $NaAlH_4$.[8,11,12] Significant experimental[13−17] and theoretical[11,12,18,19] works have been done to understand the mechanism of desorption of hydrogen from doped $NaAlH_4$.

Over the past, substantial efforts have been put forward to modulate the dissociation temperature, rehydrogenation mechanism, and reaction kinetics along with understanding the process of diffusion and decomposition by substituting Na/Al with a suitable transition metal (TM) dopant.[12,14,16,18,20−23] It is shown that TM atom has the capability to accommodate a large number of hydrogen atoms.[24−26] This facilitates the softening and breaking of bond between Al and H, which in turn helps the release of H_2 from $NaAlH_4$.[14] Because the TM atoms drag hydrogen atoms of the system, it yields various types of H-related defects. The latter is believed to be the reason for improved H-storage capacity.[14,15]

The charged defect in $NaAlH_4$ is a topic that has been studied in the past.[23,27] The observed defects are either Na/Al substitutional defects by TMs or simple H-related defects (viz. vacancy or interstitial). However, no quantitative information has been provided so far to understand which structures/compositions/defects are stable at what experimental conditions.[8,11,23] This is due to the fact that all theoretical calculations to understand the stability of such defects are limited to estimation of the formation energies without consideration of the environmental effects, i.e., neglecting any influence due to temperature (T) and partial pressure of H_2 (p_{H_2}) relevant for the experiment. Note that the properties of material change drastically under operational environment especially in an atmosphere of reactive molecules (here H_2).[28] Hence, its identification and control is experimentally very challenging. An indigenous combination of several experimental tools is mandatory, which is undoubtedly rare. Note that the formation energy of one isolated defect can be reduced by several electronvolts, when the defect traps a charge carrier (hole or electron) that are available in the material. This factor highly depends on the environmental conditions that is T, p_{H_2}. Thus, disentangling the relative stability of different types of charged defects at a given T, p_{H_2} is important. In this situation, it is therefore important to provide theoretical guidance to the

Received: September 5, 2018
Revised: November 23, 2018
Published: December 14, 2018

DOI: 10.1021/acs.jpcc.8b08687
J. Phys. Chem. C 2019, 123, 62−69

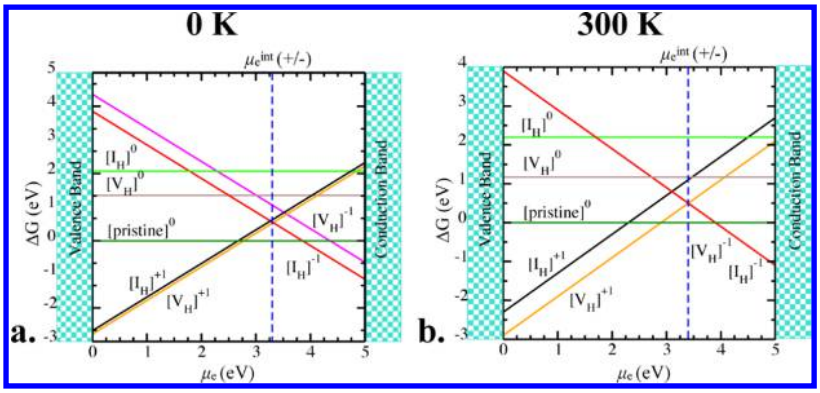

Figure 1. Phase diagram at (a) T = 0 K and (b) T = 300 K showing the Gibbs free energy of formation ($\Delta G(T,p_{H_2})$) of hydrogen-related charged defects as a function of μ_e at p_{H_2} = 1 atm. μ_e^{int} represents the value of intrinsic μ_e.

experiment regarding thermodynamic stability of different dopants as a function of charges at a realistic condition.

In this article, our aim is to elucidate the importance of environmental effects (i.e., T, p_{H_2}) to find the thermodynamic stability of different defects. Our material of choice is $NaAlH_4$—an important hydrogen storage material and a widely studied prototypical system.[8,16,20,22] We have employed state-of-the-art methodologies, viz. density-functional theory (DFT)[29] and ab initio atomistic thermodynamics,[30,31] to revisit the case of TM doped complex metal hydrides at a realistic condition. From the thermodynamic stability of different H related defects (viz. substitution and interstitial) at a realistic condition, we validate that the inclusion of the effect of T and p_{H_2} is absolutely indispensable, where DFT alone quantitatively predicts totally wrong stable phases even at moderately low temperature. Note that, aiming toward a better desorption kinetics, various TM atoms (viz. Cd, Zn, Sc, Ni, Pd, and Ti) are experimentally doped in past in $NaAlH_4$.[13−16,18,22,32−37] However, a clear microscopic understanding at the atomistic level to explore a suitable TM dopant at a realistic condition to modulate the dehydrogenation kinetics is lacking. Here, we also provide a thorough procedure to identify the most suitable dopants that may be more effective for a better desorption kinetics in $NaAlH_4$.

COMPUTATIONAL DETAILS

The DFT calculations are performed using FHI-aims, which is an all-electron code that uses numeric-atom-centered basis set.[38] The supercell size of the model structure of $NaAlH_4$ has been kept on increasing until the single defect state becomes fully localized. Our converged supercell contains 96 atoms (i.e., $Na_{16}Al_{16}H_{64}$). All the structures were fully relaxed up to 0.01 meV/Å force minimization using the Broyden−Fletcher−Goldfarb−Shanno algorithm under periodic boundary conditions. The total energy tolerance is set at 0.001 meV. The k-mesh was converged and kept fixed at 8 × 8 × 8 k-mesh size. All the calculations are done using tight/tier2-settings as implemented in FHI-aims.[38] It has been shown already that generalized gradient approximation yields accurate results for this class of materials.[23,27,39] Thus, we have used Perdew−Burke−Ernzerhof[40] functional for the treatment of exchange and correlations (ϵ_{xc}). Because this material operates at finite temperature (~300−350 K), the environmental effect is included in the expression of total DFT energy by adding the free energy of formation due to lattice vibrations. The energy of phonons is calculated within the harmonic approximation using the Phonopy code[41] for the postprocessing of the harmonic force constants generated by the finite displacement method. The configurational entropy term due to rearrangement of defects is also taken care of as in ref 42.

RESULTS

Formation Energy of Hydrogen-Related Defects. As a first step, the Gibbs free energy of formation ($\Delta G(T,p_{H_2})$) of H-related defects [i.e., hydrogen-vacancy (V_H) and hydrogen-interstitial (I_H) defects in 96-atom supercell] in $NaAlH_4$ is calculated using the following formula:[30,43,44]

$$\Delta G(T,p_{H_2}) = \Delta E_f(T) - x\mu_H(T,p_{H_2}) + q(\mu_e + \mathrm{VBM} + \Delta) \quad (1)$$

where ΔE_f is the difference in the free energies of defected supercell and pristine supercell. It is equal to $[E(Na_{16}Al_{16}H_{65})]^q - [E(Na_{16}Al_{16}H_{64})]^0$ for $[I_H]^q$ defect, whereas $[E(Na_{16}Al_{16}H_{63})]^q - [E(Na_{16}Al_{16}H_{64})]^0$ for $[V_H]^q$ defect. Here, total DFT energy is added with the free energy of vibrations estimated from Phonopy at a given T. The value of x depends on the type of defect. It takes a positive value if atoms are added to the system and a negative value for atoms being removed from the system. Therefore, here, it is equal to +1 for $[I_H]^q$ defects and −1 for $[V_H]^q$ defects. q is the number of electrons added or removed from the system. If an electron is removed from the system it is +1, whereas if an electron is added, it is −1. μ_e is the chemical potential of electron with respect to the valence band maximum (VBM) and Δ is the difference in core levels of defected and pristine neutral supercells. μ_H is the chemical potential of hydrogen atom. μ_H can be computed as $1/2\mu_{H_2}$, where the latter is calculated as [see details of this methodology in ref 30]

$$\mu_{H_2}(T, p_{H_2}) = -k_BT \ln\left[\left(\frac{2\pi m}{h^2}\right)^{3/2}(k_BT)^{5/2}\right] + k_BT \ln p_{H_2} - k_BT \ln\left[\frac{8\pi^2 I k_BT}{h^2}\right] + \frac{h\nu_{HH}}{2} + k_BT \ln\left[1 - \exp\left[-\frac{h\nu_{HH}}{k_BT}\right]\right] + E^{DFT}(H_2) - k_BT \ln J + k_BT \ln \sigma \quad (2)$$

Here, T, p_{H_2}, k_B, h, and ν_{HH} are respectively the temperature, partial pressure of hydrogen, Boltzmann constant, Planck

DOI: 10.1021/acs.jpcc.8b08687
J. Phys. Chem. C 2019, 123, 62−69

constant, and zero point frequency of vibration of H_2 molecule. m and I are respectively the mass and moment of inertia of the molecule. J and σ denote spin and symmetry of the molecule, respectively.

Now, μ_{H_2} should be defined with respect to some reference. Here, our μ_{ref} is $E^{DFT}(H_2) + \frac{h\nu_{HH}}{2}$. The latter term is called the zero-point energy of H_2. Therefore, $\Delta\mu_{H_2}$ can be written as

$$\mu_{H_2}(T, p_{H_2}) = \mu_{H_2}(T, p_{H_2}) - \mu_{ref} + \mu_{ref}$$
$$= \Delta\mu_{H_2}(T, p_{H_2}) + E^{DFT}(H_2) + \frac{h\nu_{HH}}{2}$$

$$\Delta\mu_{H_2}(T, p_{H_2}) = \mu_{H_2}(T, p_{H_2}) - \left[E^{DFT}(H_2) + \frac{h\nu_{HH}}{2}\right] \quad (3)$$

Note that if $\Delta\mu_{H_2}$ is set to zero and on neglecting the vibrational free energy contribution in the eqs 1 and 2, this will yield the same results as shown by Peles and Van de Walle.[23] However, in order to comment on the stability of different H-related defects at realistic environmental conditions, it is necessary to take the effect of T and p_{H_2} into eqs 1 and 2. On doing so, we obtain totally different results. In Figure 1, $\Delta G(T,p_{H_2})$ is shown as a function of μ_e for various H-related defects (viz. H-vacancy $[V_H]^q$ and H-interstitial $[I_H]^q$) in $NaAlH_4$ at two different conditions. In Figure 1a, while estimating $\Delta G(T,p_{H_2})$ only DFT energetics are considered, whereas in Figure 1b, the effect of T and p_{H_2} is included by adding the DFT energetics with the free energy contribution due to lattice vibration at T = 300 K and p_{H_2} = 1 atm. We find from Figure 1a that at 0 K (i.e., DFT energetics only), for μ_e positioned near conduction band minimum (CBm), $[I_H]^{-1}$ is the predominant defect state having minimum $\Delta G(T,p_{H_2})$. However, if we do the same analysis at T = 300 K and p_{H_2} = 1 atm, we find two competing defects viz. $[I_H]^{-1}$ and $[V_H]^{-1}$, having same $\Delta G(T,p_{H_2})$ (see Figure 1b). Therefore, in order to visualize the effect of T and p_{H_2} simultaneously, we have shown three-dimensional (3D) phase diagrams (see Figure 2) at various T (viz. 50, 200, 300, and 400 K) and p_{H_2} range from 10^{-5} to 1 atm. Here, on x-axis $\Delta\mu_H$ is varied in accordance with the corresponding T and p_{H_2}. On y-axis μ_e is varied from VBM to CBm of $NaAlH_4$. On z-axis the negative $\Delta G(T,p_{H_2})$ values are plotted so that only the most stable phases are visible from the top. We find from Figure 2 that on further increasing T, at $\mu_e \geq$ 3.8 for all the values of the considered range of p_{H_2}, instead of $[I_H]^{-1}$, $[V_H]^{-1}$ becomes the most stable defect having minimum $\Delta G(T,p_{H_2})$. Therefore, this finding validates that consideration of the environmental effect is absolutely important for this class of materials. DFT even with appropriate ϵ_{xc} functionals fails to predict the stable phases of $NaAlH_4$ at a finite T and p_{H_2}.

Concentration of Hydrogen-Related Defects. In order to ensure the validity of our above analysis, we estimate the concentration of different defects with varying T at a constant p_{H_2} = 1 atm. For a large size of supercell such that the interaction among defects is negligible, the defects should follow Fermi Dirac statistics.[43,45] Let us assume that N is the total number of

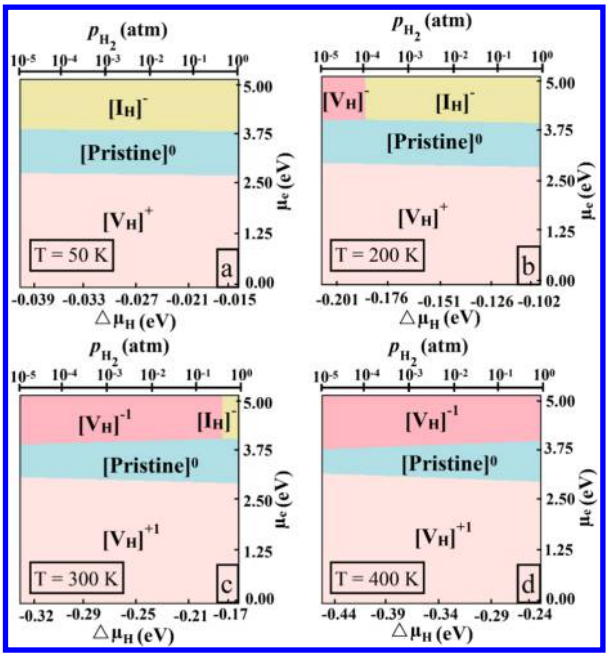

Figure 2. 3D phase diagram showing the stable phases (with minimum $\Delta G(T,p_{H_2})$) of hydrogen-related charged defects as a function of μ_e and $\Delta\mu_H$ at different temperatures: (a) T = 50 K, (b) T = 200 K, (c) T = 300 K, and (d) T = 400 K. On x-axis, $\Delta\mu_H$ is varied in accordance with T and p_{H_2} conditions, while on y-axis μ_e is varied from VBM to CBm. Colored surfaces are the projections of the stable phases having minimum $\Delta G(T,p_{H_2})$ at those environmental conditions.

all possible defect sites in the lattice, and N_n and N_p are the total number of type-n and type-p defects with ΔG_n and ΔG_p as the Gibbs free energy of formation, respectively. Therefore, we can write

$$N_n = \left(N - \sum_{n\neq k} N_k\right)\frac{1}{1 + \exp\left[\frac{\Delta G_n}{k_B T}\right]}$$
$$N_p = \left(N - \sum_{p\neq k} N_k\right)\frac{1}{1 + \exp\left[\frac{\Delta G_p}{k_B T}\right]} \quad (4)$$

Combining the above two coupled equations, we get

$$\frac{N_n}{N_p} = \exp\left[\frac{\Delta G_p - \Delta G_n}{k_B T}\right] \quad (5)$$

Expressing this in the form of N, we calculate the concentration (C_n) of type-n defects as follows:

$$C_n = \frac{N_n}{N} = \frac{\exp\left[-\frac{\Delta G_n}{k_B T}\right]}{1 + \sum_{p\neq n}\exp\left[-\frac{\Delta G_p}{k_B T}\right]} \quad (6)$$

Figure 3 represents the concentration of various H-related defects in $NaAlH_4$ plotted as a function of T at p_{H_2} = 1 atm and μ_e is at CBm. We see that at about 300 K the defect state with the highest concentration value switches from $[I_H]^-$ to $[V_H]^-$. At lower temperatures, $[I_H]^-$ has the maximum defect concentration, whereas later on increasing T, $[V_H]^-$ slowly starts dominating over $[I_H]^-$. This further quantitatively validates the

DOI: 10.1021/acs.jpcc.8b08687
J. Phys. Chem. C 2019, 123, 62−69

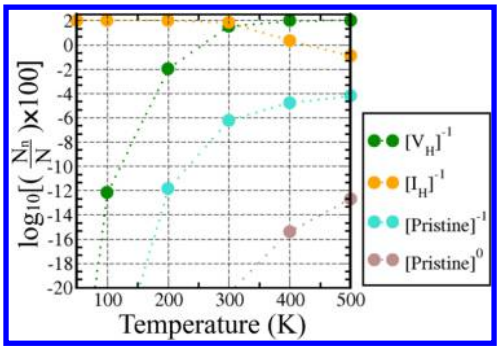

Figure 3. Logarithm of concentration (in %) of H-related charged defects plotted as a function of T. The value on y-axis 2 corresponds to 100% concentration of a particular defect in the supercell. p_{H_2} is fixed at 1 atm and μ_e is set at the CBm. For T < 300 K, the concentration of $[I_H]^{-1}$ is ∼100%, whereas for T > 300 K the concentration of $[V_H]^{-1}$ is ∼100%.

initial analysis (discussed previously) on the thermodynamic stability of various H-related defects at a realistic condition. From here, we can conclude that in order to capture the most favorable intrinsic defect states in metal hydrides, one should not rely only on DFT energetics.[a] Inclusion of environmental effects to the free energy of formation is very crucial and cannot be neglected even at a moderately low temperature.

TM Dopants in $NaAlH_4$ for a Better Desorption Kinetics. The reason of low reaction kinetics and high dissociation temperature of $NaAlH_4$ is the strong covalent bonds between Al and H atoms. TM atoms, when doped in $NaAlH_4$, are believed to enhance the reaction kinetics as well as lowering the dissociation temperatures. However, this depends on three of the basic factors to justify if the chosen TM dopant is capable to modulate the desorption kinetics or not. First, this is due to the presence of unfilled d-orbitals which can accommodate electrons from the nearby H-atoms of the $[AlH_4]^-$ complex. It is therefore important to analyze the effect of different TM dopants to distort the bond lengths between Al and H atoms in the $[AlH_4]^-$ complex. Note that, to have a lowered desorption temperature, the TM−H bond strength should also not be strong enough so that the H atoms just shift their position from Al to TM. Second, the thermodynamic stability of the TM dopants in a material at a realistic condition is also an important factor to determine if doping with the concerned TM is at all possible or not at a given experimental condition. This also gives us an idea regarding the dopant's preferred lattice site and charge state. This is achieved by calculating the $\Delta G(T,p_{H_2})$ for different dopants as a function of μ_e. The configuration corresponding to the minimum value of $\Delta G(T,p_{H_2})$ is considered to be the most stable configuration. Finally, it is believed that the mechanism of dehydrogenation from $NaAlH_4$ involves self-diffusion of various intrinsic defects, for example $[I_H]^q$ and $[V_H]^q$.[12,16,23] It is therefore obvious that if a defect has higher concentration in a material, it diffuses more through the material. Therefore, by addition of a TM dopant, one has to estimate the change in $\Delta G(T,p_{H_2})$ of those intrinsic H-related defects. If $\Delta G(T,p_{H_2})$ is reduced further on doping, this will lead to increase the concentration of the respective defects as well, thereby a better desorption is expected and vice versa. Taking all these three factors in account in the next section, we have tried to understand the most suitable TM dopant in $NaAlH_4$ for a better desorption kinetics.

Structural Distortion Created by TM Dopants. On doping with a TM atom, we have noticed the elongation of Al−H bond in the $[AlH_4]^-$ complex in $NaAlH_4$. The TM atoms, with unfilled or partially filled d-orbitals, have the tendency to share electrons from the neighboring H-atoms, which in turn weakens the Al−H bond via Kubas-type interaction.[24,26,46] Thus, apparently, doping $NaAlH_4$ by TMs may ease the release of hydrogen from the material. However, for the case of Zn and Cd doping, substituted at the Na-site, there is no significant interaction between the dopant atom and the neighboring H atoms. Thus, in both the cases, the $[AlH_4]^-$ tetrahedron remains totally undistorted. This situation is not much different when Zn or Cd is doped at the Al site. This behavior of Zn and Cd may be attributed to the fully filled d-orbitals. Note that the equilibrium Al−H bond-length in $[AlH_4]^-$ is 1.64 Å. Therefore, the structural distortion of $[AlH_4]^-$ tetrahedron for better desorption highly depends on the electronic structure of the doped TM atoms. In Figure 4, we have shown the bond

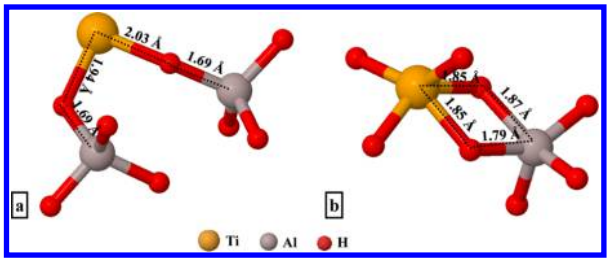

Figure 4. Ti−H and Al−H bonds in Ti-doped $NaAlH_4$. (a) Ti_{Na} configuration and (b) Ti_{Al} configuration.

elongations when Ti is doped at the Na/Al site in $NaAlH_4$. In Table 1, we provide all such structural details to establish that Sc, Ti, and Ni TMs are more capable to distort the $[AlH_4]^-$ complex than Zn, Cd, and Pd TMs.

Formation Energy of TM Dopants. Next, we substitute various TM atoms (viz. Cd, Zn, Sc, Ni, Pd, Ti) separately either at Na or Al site in the supercell of $NaAlH_4$ (i.e., $Na_{16}Al_{16}H_{64}$) to estimate its Gibbs free energy of formation $[\Delta G(TM_{Na/Al})]^q$ as a function of different charge state q. This is expressed by the following two equations:

Table 1. Table of Bond Lengths for the Bonds between Al and H as well as for the Bonds between TM and H after Doping

	bond length (Å)	
type of dopants	Al−H	TM−H
Cd_{Al}	1.65	1.79
Cd_{Na}	1.65	2.46[a]
Zn_{Al}	1.65	1.62
Zn_{Na}	1.65	2.40[a]
Sc_{Al}	1.65	1.92
Sc_{Na}	1.70	2.09
Ni_{Al}	1.81	1.51
Ni_{Na}	1.72	1.75
Pd_{Al}	1.65	1.63
Pd_{Na}	1.72	1.86
Ti_{Al}	1.79	1.84
Ti_{Na}	1.69	1.94

[a]No bond is formed with the neighboring H-atoms. The numbers correspond to the distance between TM atom and the nearest H-atom.

DOI: 10.1021/acs.jpcc.8b08687
J. Phys. Chem. C 2019, 123, 62−69

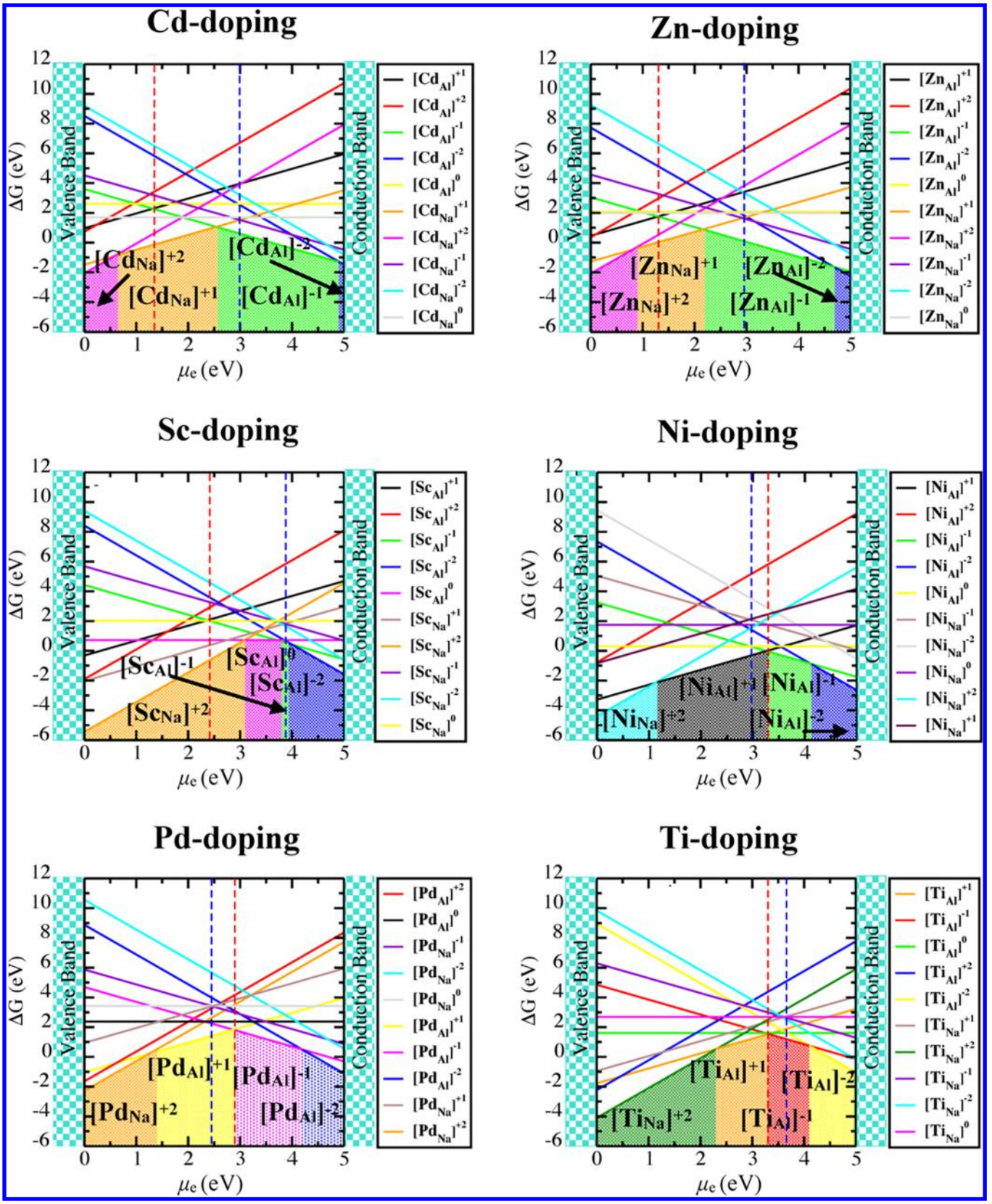

Figure 5. Formation energy of TM (Cd, Zn, Sc, Ni, Pd, Ti)-substituted $NaAlH_4$ as a function of μ_e at various electronic charge states q (−2, −1, 0, +1, +2). $[TM_{Al}]^q$ and $[TM_{Na}]^q$ denote TM atom substituted at the position of Al or Na, respectively, with charge q. The colored regions represent the respective most stable defect states having minimum E_f as a function of μ_e. The vertical lines are drawn to highlight the position of μ_e (Fermi-level), at which thermodynamic transition between negative and positive charges takes place. Red colored line represents the position of Fermi-level for $[TM_{Al}]^{+1} \rightarrow [TM_{Al}]^{-1}$ transition, whereas blue colored line represents the same for $[TM_{Na}]^{+1} \rightarrow [TM_{Na}]^{-1}$.

DOI: 10.1021/acs.jpcc.8b08687
J. Phys. Chem. C 2019, 123, 62−69

$$[\Delta G(TM_{Na})]^q = [E(Na_{15}Al_{16}H_{64}TM)]^q - [E(Na_{16}Al_{16}H_{64})]^0 + E^{DFT}(Na) - E^{DFT}(TM) + q(\mu_e + VBM + \Delta) \quad (7)$$

$$[\Delta G(TM_{Al})]^q = [E(Na_{16}Al_{15}H_{64}TM)]^q - [E(Na_{16}Al_{16}H_{64})]^0 + E^{DFT}(Al) - E^{DFT}(TM) + q(\mu_e + VBM + \Delta) \quad (8)$$

Here, $[E(Na_{15}Al_{16}H_{64}TM)]^q$ and $[E(Na_{16}Al_{15}H_{64}TM)]^q$ are free energies of the supercell $TMNa_{15}Al_{16}H_{64}$ and $TMNa_{16}Al_{15}H_{64}$ at a charge state q. $[E(Na_{16}Al_{16}H_{64})]^0$ is the free energy of the neutral pristine supercell $Na_{16}Al_{16}H_{64}$. μ_e is the chemical potential referenced with respect to VBM. Δ is the core alignment between the neutral pristine supercell and the one with charged defect. The total energies of single Na-atom $[E^{DFT}(Na)]$, Al-atom $[E^{DFT}(Al)]$ and TM-atoms $[E^{DFT}(TM)]$ are taken from the energies of their respective bulk forms.

In Figure 5, we show the formation energy of various charged defects (i.e., TM substitution either at Na (TM_{Na}) or Al (TM_{Al}) site). This illustrates the type of charged dopants to be stable in $NaAlH_4$. The enhanced stability of a specific q value for the case of a specific $[TM_{Na}]^q$ or $[TM_{Al}]^q$ configuration can be explained on the basis of electronic structure of the respective TM atoms. Note that the electronic configuration of cadmium (Cd) is $[Kr]4d^{10}5s^2$. Because of the presence of the full filled d-orbital, apparently it has one electron more than Na in the valence shell. Thus, Cd_{Na} is expected to act as a donor level and can be stable either in $[Cd_{Na}]^0$ or in $[Cd_{Na}]^{+1}$ charge state. On the other hand, Cd-atom has one valence electron less than Al-atom. Therefore, Cd_{Al} is expected to act as an acceptor level and can be stable either in $[Cd_{Al}]^0$ or in $[Cd_{Al}]^{-1}$ charge state (see Figure 5). The same explanation holds for zinc (Zn) doping (electronic configuration $[Ar]3d^{10}4s^2$) as well. Therefore, the substitution of Zn at the place of Na should behave as a donor level, whereas substitution of Zn at the place of Al should behave as an acceptor level. Hence, $[Zn_{Na}]^{+1}$ is expected to be the most stable defect state near valence band, whereas $[Zn_{Al}]^{-1}$ is to be the most stable defect state near conduction band. Now for the case of scandium (Sc) (electronic configuration $[Ar]3d^14s^2$), it has two electrons more than Na in the valence shell. Hence, replacing Na with Sc is expected to be a donor level. Thus, $[Sc_{Na}]^{+2}$ should be the most favorable configuration near valence band. However, Sc has exactly the same number of valence electrons as Al does. This clearly justifies the stability of $[Sc_{Al}]^0$. However, this situation is intriguing if the dopant is having the possibility of possessing multiple valency due to the presence of excess number of valence electrons in its d-orbital. This is the case for nickel (Ni: electronic configuration $[Ar]3d^84s^2$), palladium (Pd: electronic configuration $[Kr]4d^{10}$) and titanium (Ti: electronic configuration $[Ar]3d^24s^2$), where substitution of Na with +2 charge state is favored when the material is highly p-doped. Otherwise, substitution of Al is favored with +1, −1, and −2 charge states depending on the value of μ_e. From the formation energy diagram as shown in Figure 5, we infer that substitution of early TMs (viz. Sc, Ti, and Ni) is energetically more favorable as compared to late TMs (viz. Zn, Cd, and Pd).

Position of Charge Transition Level $\epsilon(\pm)$ Due to the External TM Dopants and Its Effect on Self-Diffusion of H-Related Defects. Note that while estimating the concentrations of charged defects, they are usually governed by charge neutrality condition

$$\sum_i q_i \times C_i - n_e + n_h = 0 \quad (9)$$

Referring to eq 6, C_i is the concentration of the ith defect. Thus, the first term of the above equation is the net charge due to all possible defects, which should be compensated by the free carriers (either electrons or holes) present in the material. n_e and n_h are the concentration of electrons and holes in the conduction band and valence band, respectively. Because $NaAlH_4$ is a wide-band-gap semiconductor, the concentrations of free carriers are usually very small. Therefore, the charge neutrality condition is satisfied by incorporation of various defects with opposite charges. In view of this, it is more relevant to see those point defects and dopants that create defect levels deep in the band gap. This causes the resulting μ_e (Fermi-level) position to be neither close to CBm nor VBM. This further justifies the reason of neglecting the terms n_e and n_h to be ∼zero in eq 9. Note that the defects with lowest ΔG are the highest in C. These are the dominant C_is in eq 9. We now define the thermodynamic transition state, $\epsilon(\pm)$, as the position of Fermi-level (i.e., a specific value of μ_e), at which positive and negative charged defect states have equal ΔG values. If there are no dopants added in $NaAlH_4$, the μ_e position is determined by the intrinsic defects (viz. $[V_H]^q$ and $[I_H]^q$). The value of μ_e^{int} is therefore 3.32 eV at 0 K and 3.40 eV at 300 K (see Figure 1). At this value of μ_e^{int}, the ΔG values of most stable defect configurations become equal. As described in refs 23 and 39, the presence of extrinsic impurities alters the value of μ_e, which as a consequence affects the stability and diffusion of intrinsic H-related defects.

In Table 2, we have given $\Delta\mu_e(=\epsilon(\pm) - \mu_e^{int})$ values for all the considered doping configurations. From the amount by which μ_e is shifted for a particular dopant, we can qualitatively estimate the effect of that dopant on the reaction kinetics. If the shift in μ_e, that is, $\Delta\mu_e > 0$, or say, is shifted toward right, the ΔG of the predominant intrinsic impurity will decrease in the presence of that particular dopant. This will increase the concentration and hence the self-diffusion of intrinsic impurity. Thus, that doping configuration can be considered suitable for improving the reaction kinetics in the material. On the contrary, if $\Delta\mu_e < 0$ for a

Table 2. Table of $\Delta\mu_e = \epsilon(\pm) - \mu_e^{int}$ in (eV) Values at Temperatures 0 and 300 K for Various Doping Configurations[a]

	$\Delta\mu_e$ (eV)	
type of dopants	T = 0 K	T = 300 K
Cd_{Al}	−1.99	−2.07
Cd_{Na}	−0.30	−0.38
Zn_{Al}	−2.02	−2.10
Zn_{Na}	−0.38	−0.46
Sc_{Al}	−0.97	−1.05
Sc_{Na}	0.54	0.46
Ni_{Al}	−0.05	−0.13
Ni_{Na}	−0.37	−0.45
Pd_{Al}	−0.43	−0.51
Pd_{Na}	−0.83	−0.91
Ti_{Al}	0.00	−0.08
Ti_{Na}	0.27	0.19

[a] TM_{Al} and TM_{Na} denote TM doped at position of Al and Na, respectively, where TM = Cd, Zn, Sc, Ni, Pd, Ti.

DOI: 10.1021/acs.jpcc.8b08687
J. Phys. Chem. C 2019, 123, 62−69

dopant, that dopant is not considered to be a suitable choice in order to improve the reaction kinetics. In Figure 5, we have shown vertical dashed lines to highlight the positions of μ_e for different doping configurations (see the red colored lines for TM_{Al} defects and blue colored line for TM_{Na} defects). From Table 2, we can conclude that the most favorable choice of dopant in view of improving reaction kinetics in $NaAlH_4$ at realistic environmental conditions may be Sc_{Na}, Ti_{Na}, and Ti_{Al}. However, from our analysis, Ti_{Na} is expected to be a better choice than Ti_{Al} at the operational environmental conditions of the material. We see that at 300 K μ_e of Ti_{Al} shifts toward left ($\Delta\mu_e < 0$), which makes it an unsuitable doping configuration at realistic conditions (T = 300 K, p_{H_2} = 1 atm). Therefore, from Table 2, we can conclude that the most favorable choice of dopant in view of improving reaction kinetics in $NaAlH_4$ at realistic environmental conditions may be Sc_{Na} and Ti_{Na}.

CONCLUSIONS

In summary, we have tried to understand the role of charged defect in TM-doped complex metal hydrides at a realistic condition using DFT combined with ab initio atomistic thermodynamics. Our choice of materials is $NaAlH_4$—a prototypical system for hydrogen storage material. We show that the role of environmental effect is extremely important so that DFT with reasonable ϵ_{xc} functional fails to capture the correct stable phases even at moderately low temperatures. From our analysis, we find $[V_H]$ is the most abandoned defect in $NaAlH_4$ at a realistic condition. We have also given a thorough methodological procedure to find the most suitable TM dopant for a better desorption in $NaAlH_4$. We show that for TM substitution, Na-site in $NaAlH_4$ is more suitable from the perspective of having enhanced self-diffusion due to H-related defects. Finally, we correlate why Sc and Ti are supposed to be the best dopants for this system.

AUTHOR INFORMATION

Corresponding Authors

*E-mail: Ekta.Arora@physics.iitd.ac.in (E.A.).
*E-mail: saswata@physics.iitd.ac.in. Phone: +91-2659 1359. Fax: +91-2658 2037 (S.B.).

ORCID

Saswata Bhattacharya: 0000-0002-4145-4899

Notes

The authors declare no competing financial interest.

ACKNOWLEDGMENTS

S.B. and E.A. acknowledge the financial support from YSS-SERB research grant, DST, India (grant no. YSS/2015/001209). S.S. acknowledges CSIR, India, for the senior research fellowship [grant no. 09/086(1231)2015-EMR-I]. P.B. acknowledges UGC, India, for the junior research fellowship [grant no. 20/12/2015(ii)EU-V]. M.K. acknowledges CSIR, India, for the junior research fellowship [grant no. 09/086(1292)2017-EMR-I]. We acknowledge the High Performance Computing (HPC) facility at IIT Delhi for computational resources.

ADDITIONAL NOTE

[a]By DFT energetics, we mean the total ground state energies obtained from DFT without including phonon energy and effect of temperature and partial pressure of hydrogen in the energy of gaseous molecule of hydrogen.

REFERENCES

(1) Ichikawa, T.; Hanada, N.; Isobe, S.; Leng, H.; Fujii, H. Mechanism of Novel Reaction from LiNH2and LiH to Li2NH and H2as a Promising Hydrogen Storage System. *J. Phys. Chem. B* **2004**, *108*, 7887−7892.

(2) Sakintuna, B.; Lamaridarkrim, F.; Hirscher, M. Metal hydride materials for solid hydrogen storage: A review☆. *Int. J. Hydrogen Energy* **2007**, *32*, 1121−1140.

(3) Schüth, F.; Bogdanović, B.; Felderhoff, M. Light metal hydrides and complex hydrides for hydrogen storage. *Chem. Commun.* **2004**, 2249−2258.

(4) Bhattacharya, S.; Wu, G.; Ping, C.; Feng, Y. P.; Das, G. P. Lithium Calcium Imide [Li2Ca(NH)2] for Hydrogen Storage: Structural and Thermodynamic Properties. *J. Phys. Chem. B* **2008**, *112*, 11381−11384.

(5) Bhattacharya, S.; Xiong, Z.; Wu, G.; Chen, P.; Feng, Y. P.; Majumder, C.; Das, G. P. Dehydrogenation Mechanism of Mono-ammoniated Lithium Amidoborane [Li(NH3)NH2BH3]. *J. Phys. Chem. C* **2012**, *116*, 8859−8864.

(6) Schlapbach, L.; Züttel, A. *Materials For Sustainable Energy: A Collection of Peer-Reviewed Research and Review Articles from Nature Publishing Group*; World Scientific, 2011; pp 265−270.

(7) Orimo, S.-i.; Nakamori, Y.; Eliseo, J. R.; Züttel, A.; Jensen, C. M. Complex hydrides for hydrogen storage. *Chem. Rev.* **2007**, *107*, 4111−4132.

(8) Peles, A.; Alford, J. A.; Ma, Z.; Yang, L.; Chou, M. Y. First-principles study of $NaAlH_4$and Na_3AlH_6complex hydrides. *Phys. Rev. B: Condens. Matter Mater. Phys.* **2004**, *70*, 165105.

(9) Vegge, T. Equilibrium structure and Ti-catalyzed H2 desorption in NaAlH4 nanoparticles from density functional theory. *Phys. Chem. Chem. Phys.* **2006**, *8*, 4853−4861.

(10) Dathar, G. K. P.; Mainardi, D. S. Kinetics of Hydrogen Desorption in NaAlH4 and Ti-Containing NaAlH4. *J. Phys. Chem. C* **2010**, *114*, 8026−8031.

(11) Gunaydin, H.; Houk, K. N.; Ozolins, V. Vacancy-mediated dehydrogenation of sodium alanate. *Proc. Natl. Acad. Sci. U.S.A.* **2008**, *105*, 3673−3677.

(12) Wilson-Short, G. B.; Janotti, A.; Hoang, K.; Peles, A.; Van de Walle, C. G. First-principles study of the formation and migration of native defects in $NaAlH_4$. *Phys. Rev. B: Condens. Matter Mater. Phys.* **2009**, *80*, 224102.

(13) Weidenthaler, C.; Pommerin, A.; Felderhoff, M.; Bogdanović, B.; Schüth, F. On the state of the titanium and zirconium in Ti- or Zr-doped NaAlH4hydrogen storage material. *Phys. Chem. Chem. Phys.* **2003**, *5*, 5149−5153.

(14) Íñiguez, J.; Yildirim, T.; Udovic, T. J.; Sulic, M.; Jensen, C. M. Structure and hydrogen dynamics of pure and Ti-doped sodium alanate. *Phys. Rev. B: Condens. Matter Mater. Phys.* **2004**, *70*, 060101.

(15) Fichtner, M.; Fuhr, O.; Kircher, O.; Rothe, J. r. Small Ti clusters for catalysis of hydrogen exchange in NaAlH4. *Nanotechnology* **2003**, *14*, 778.

(16) Lohstroh, W.; Fichtner, M. Rate limiting steps of the phase transformations in Ti-doped $NaAlH_4$ investigated by isotope exchange. *Phys. Rev. B: Condens. Matter Mater. Phys.* **2007**, *75*, 184106.

(17) Gross, K. J.; Guthrie, S.; Takara, S.; Thomas, G. In-situ X-ray diffraction study of the decomposition of NaAlH4. *J. Alloys Compd.* **2000**, *297*, 270−281.

(18) Chaudhuri, S.; Muckerman, J. T. First-principles study of Ti-catalyzed hydrogen chemisorption on an Al surface: a critical first step for reversible hydrogen storage in NaAlH4. *J. Phys. Chem. B* **2005**, *109*, 6952−6957.

(19) Ke, X.; Tanaka, I. Decomposition reactions for $NaAlH_4$, Na_3AlH_6, and NaH: First-principles study. *Phys. Rev. B: Condens. Matter Mater. Phys.* **2005**, *71*, 024117.

(20) Bogdanović, B.; Schwickardi, M. Ti-doped alkali metal aluminium hydrides as potential novel reversible hydrogen storage materials. *J. Alloys Compd.* **1997**, *253*, 1−9.

(21) Bhattacharya, S.; Bhattacharya, A.; Das, G. P. Anti-kubas type interaction in hydrogen storage on a Li decorated BHNH sheet: a first-principles based study. *J. Phys. Chem. C* **2012**, *116*, 3840−3844.

DOI: 10.1021/acs.jpcc.8b08687
J. Phys. Chem. C 2019, 123, 62−69

(22) Nielsen, T. K.; Polanski, M.; Zasada, D.; Javadian, P.; Besenbacher, F.; Bystrzycki, J.; Skibsted, J.; Jensen, T. R. Improved hydrogen storage kinetics of nanoconfined NaAlH4 catalyzed with TiCl3 nanoparticles. *ACS Nano* **2011**, *5*, 4056−4064.
(23) Peles, A.; Van de Walle, C. G. Role of charged defects and impurities in kinetics of hydrogen storage materials: A first-principles study. *Phys. Rev. B: Condens. Matter Mater. Phys.* **2007**, *76*, 214101.
(24) Bhattacharya, A.; Bhattacharya, S.; Majumder, C.; Das, G. P. Transition-metal decoration enhanced room-temperature hydrogen storage in a defect-modulated graphene sheet. *J. Phys. Chem. C* **2010**, *114*, 10297−10301.
(25) Bhattacharya, S.; Majumder, C.; Das, G. P. 3d Transition metal decorated B-C-N composite nanostructures for efficient hydrogen storage: A first-principles study. *Bull. Mater. Sci.* **2009**, *32*, 353−360.
(26) Bhattacharya, S.; Majumder, C.; Das, G. P. Hydrogen storage in Ti-Decorated BC4N nanotube. *J. Phys. Chem. C* **2008**, *112*, 17487−17491.
(27) Du, A. J.; Smith, S. C.; Lu, G. Q. Role of charge in destabilizing AlH 4 and BH 4 complex anions for hydrogen storage applications: Ab initio density functional calculations. *Phys. Rev. B: Condens. Matter Mater. Phys.* **2006**, *74*, 193405.
(28) Bhattacharya, S.; Levchenko, S. V.; Ghiringhelli, L. M.; Scheffler, M. Stability and metastability of clusters in a reactive atmosphere: Theoretical evidence for unexpected stoichiometries of mg M o x. *Phys. Rev. Lett.* **2013**, *111*, 135501.
(29) Kohn, W.; Sham, L. J. Self-consistent equations including exchange and correlation effects. *Phys. Rev.* **1965**, *140*, A1133.
(30) Bhattacharya, S.; Levchenko, S. V.; Ghiringhelli, L. M.; Scheffler, M. Efficientab initioschemes for finding thermodynamically stable and metastable atomic structures: benchmark of cascade genetic algorithms. *New J. Phys.* **2014**, *16*, 123016.
(31) Chaput, L.; Togo, A.; Tanaka, I.; Hug, G. Phonon-phonon interactions in transition metals. *Phys. Rev. B: Condens. Matter Mater. Phys.* **2011**, *84*, 094302.
(32) Liu, J.; Ge, Q. A first-principles study of Sc-doped NaAlH4 for reversible hydrogen storage. *J. Alloys Compd.* **2007**, *446*, 267−270.
(33) Bogdanović, B.; Felderhoff, M.; Pommerin, A.; Schüth, F.; Spielkamp, N. Advanced Hydrogen-Storage Materials Based on Sc-, Ce-, and Pr-Doped NaAlH4. *Adv. Mater.* **2006**, *18*, 1198−1201.
(34) Anton, D. L. Hydrogen desorption kinetics in transition metal modified NaAlH4. *J. Alloys Compd.* **2003**, *356*, 400−404.
(35) Song, Y.; Dai, J. H.; Li, C. G.; Yang, R. Influence of dopants Ti and Ni on dehydrogenation properties of NaAlH4: electronic structure mechanisms. *J. Phys. Chem. C* **2009**, *113*, 10215−10221.
(36) Li, W.-B.; Li, L.; Ren, Q.-L.; Wang, Y.-J.; Jiao, L.-F.; Yuan, H.-T. Ni-B-doped NaAlH4 hydrogen storage materials prepared by a facile two-step synthesis method. *Rare Met.* **2013**, *34*, 679−682.
(37) Wang, H.; Tezuka, A.; Ogawa, H.; Ikeshoji, T. NaAlH 4 doped with Ti or Sc: Bulk and surface investigation from first principles. *Phys. Rev. B: Condens. Matter Mater. Phys.* **2011**, *83*, 045112.
(38) Blum, V.; Gehrke, R.; Hanke, F.; Havu, P.; Havu, V.; Ren, X.; Reuter, K.; Scheffler, M. Ab initio Molecular Simulations with Numeric Atom-centered Orbitals. *Comput. Phys. Commun.* **2009**, *180*, 2175−2196.
(39) Van de Walle, C. G.; Neugebauer, J. First-principles calculations for defects and impurities: Applications to III-nitrides. *J. Appl. Phys.* **2004**, *95*, 3851−3879.
(40) Perdew, J. P.; Burke, K.; Ernzerhof, M. Generalized Gradient Approximation Made Simple [Phys. Rev. Lett. 77, 3865 (1996)]. *Phys. Rev. Lett.* **1997**, *78*, 1396.
(41) Togo, A.; Tanaka, I. First principles phonon calculations in materials science. *Scr. Mater.* **2015**, *108*, 1−5.
(42) Bhattacharya, A.; Bhattacharya, S. Unraveling the role of vacancies in the potentially promising thermoelectric clathrates $Ba_8Zn_xGe_{46-x-y}\square_y$. *Phys. Rev. B* **2016**, *94*, 094305.
(43) Bhattacharya, S.; Berger, D.; Reuter, K.; Ghiringhelli, L. M.; Levchenko, S. V. Theoretical evidence for unexpected O-rich phases at corners of MgO surfaces. *Phys. Rev. Mater.* **2017**, *1*, 071601.
(44) Bhattacharya, A.; Bhattacharya, S. Exploring N-Rich Phases in LixNy Clusters for Hydrogen Storage at Nanoscale. *J. Phys. Chem. Lett.* **2015**, *6*, 3726−3730.
(45) Richter, N. A.; Sicolo, S.; Levchenko, S. V.; Sauer, J.; Scheffler, M. Concentration of Vacancies at Metal-Oxide Surfaces: Case Study of MgO(100). *Phys. Rev. Lett.* **2013**, *111*, 045502.
(46) Bhattacharya, S.; Majumder, C.; Das, G. P. Ti-Decorated BC4N sheet: A planar nanostructure for high-capacity hydrogen storage. *J. Phys. Chem. C* **2009**, *113*, 15783−15787.

DOI: 10.1021/acs.jpcc.8b08687
J. Phys. Chem. C 2019, 123, 62−69